Article

Data-driven design of metal–organic frameworks for wet flue gas CO_2 capture

https://doi.org/10.1038/s41586-019-1798-7

Received: 24 August 2018

Accepted: 18 September 2019

Published online: 11 December 2019

Peter G. Boyd[1,10], Arunraj Chidambaram[1,10], Enrique García-Díez[2,10], Christopher P. Ireland[1], Thomas D. Daff[3,8], Richard Bounds[4], Andrzej Gładysiak[1], Pascal Schouwink[5], Seyed Mohamad Moosavi[1], M. Mercedes Maroto-Valer[2], Jeffrey A. Reimer[4,7], Jorge A. R. Navarro[6], Tom K. Woo[3]*, Susana Garcia[2]*, Kyriakos C. Stylianou[1,9]* & Berend Smit[1]*

Limiting the increase of CO_2 in the atmosphere is one of the largest challenges of our generation[1]. Because carbon capture and storage is one of the few viable technologies that can mitigate current CO_2 emissions[2], much effort is focused on developing solid adsorbents that can efficiently capture CO_2 from flue gases emitted from anthropogenic sources[3]. One class of materials that has attracted considerable interest in this context is metal–organic frameworks (MOFs), in which the careful combination of organic ligands with metal-ion nodes can, in principle, give rise to innumerable structurally and chemically distinct nanoporous MOFs. However, many MOFs that are optimized for the separation of CO_2 from nitrogen[4–7] do not perform well when using realistic flue gas that contains water, because water competes with CO_2 for the same adsorption sites and thereby causes the materials to lose their selectivity. Although flue gases can be dried, this renders the capture process prohibitively expensive[8,9]. Here we show that data mining of a computational screening library of over 300,000 MOFs can identify different classes of strong CO_2-binding sites—which we term 'adsorbaphores'—that endow MOFs with CO_2/N_2 selectivity that persists in wet flue gases. We subsequently synthesized two water-stable MOFs containing the most hydrophobic adsorbaphore, and found that their carbon-capture performance is not affected by water and outperforms that of some commercial materials. Testing the performance of these MOFs in an industrial setting and consideration of the full capture process—including the targeted CO_2 sink, such as geological storage or serving as a carbon source for the chemical industry—will be necessary to identify the optimal separation material.

Different strategies have been developed to mitigate the negative effects of water on the CO_2/N_2 separation selectivity in MOF materials. For example, some MOFs have open metal sites at which amines can be attached, taking advantage of the specific amine chemistry that is also used in conventional amine scrubbing[10–13]. A previous screening study[14] investigated whether MOFs could adsorb CO_2 in the presence of water, and the results suggested that such MOFs could be de novo designed. In this work, we develop a systematic strategy for the design and preparation of custom-made MOFs that can capture carbon from wet flue gases. Our design methodology is inspired by the rational design of drug molecules, in which organic molecules that fit well into the binding pocket of a protein are mined from databases of known chemicals[15,16]. The difference in our case is that the 'drug molecule' is known (that is, CO_2), but the substrate that binds it optimally (the MOF) is not. We therefore generated a library of 325,000 hypothetical MOFs, and screened each material for its CO_2/N_2 selectivity and its CO_2 working capacity. The chemical building blocks used in the generation of these materials are shown in Extended Data Figs. 1 and 2. Figure 1a shows that 8,325 hypothetical materials possess a working capacity for CO_2 greater than 2 mmol g^{-1} and a CO_2/N_2 selectivity greater than 50—performance that surpasses that of zeolite 13X under dry conditions[17].

A key part of drug design is to analyse the optimally binding molecules for a common feature or spatial arrangement of atoms at the binding site, which is known as the pharmacophore[15]. In analogy with this, we coin the term 'adsorbaphore' to describe the common pore shape and chemistry of a binding site in a MOF that provides optimal interactions to preferentially bind to a particular guest molecule, in this case CO_2. From our top-ranked 8,325 materials, we identified

[1]Laboratory of Molecular Simulation (LSMO), Institut des Sciences et Ingénierie Chimiques, Valais (ISIC), École Polytechnique Fédérale de Lausanne (EPFL), Sion, Switzerland. [2]Research Centre for Carbon Solutions (RCCS), School of Engineering and Physical Sciences, Heriot-Watt University, Edinburgh, UK. [3]Department of Chemistry and Biomolecular Science, University of Ottawa, Ottawa, Ontario, Canada. [4]Department of Chemical and Biomolecular Engineering, University of California, Berkeley, Berkeley, CA, USA. [5]Institut des Sciences et Ingénierie Chimiques (ISIC), École Polytechnique Fédérale de Lausanne (EPFL), Lausanne, Switzerland. [6]Departamento de Química Inorgánica, Universidad de Granada, Granada, Spain. [7]Materials Science Division, Lawrence Berkeley National Laboratory, Berkeley, CA, USA. [8]Present address: Department of Engineering, University of Cambridge, Cambridge, UK. [9]Present address: Department of Chemistry, Oregon State University, Corvallis, OR, US. [10]These authors contributed equally: Peter G. Boyd, Arunraj Chidambaram, Enrique García-Díez. *e-mail: twoo@uottawa.ca; S.Garcia@hw.ac.uk; kyriakos.stylianou@oregonstate.edu; berend.smit@epfl.ch

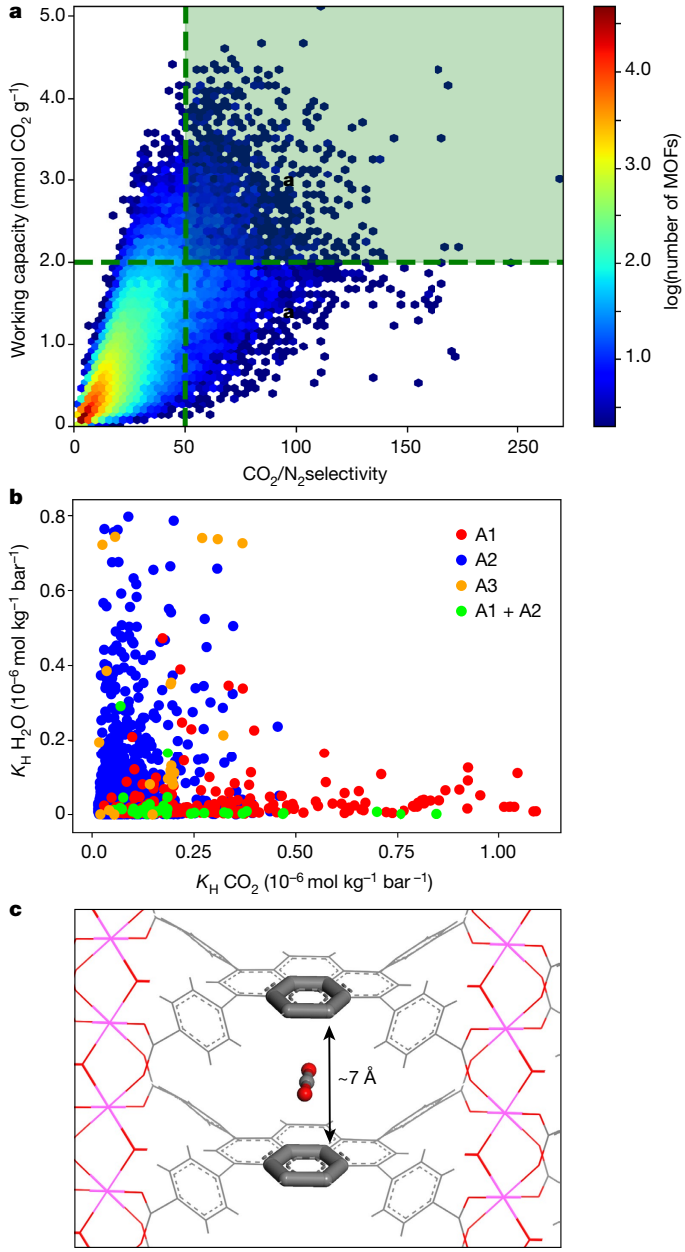


Fig. 1 | Computational screening of MOFs for strong CO_2 adsorption and selectivity. a, Results from the screening of 325,000 hypothetical MOFs under conditions that mimic post-combustion capture (adsorption at ambient temperature and 1 bar with a molar ratio of 15:85 CO_2/N_2 and regeneration at 363 K and 0.1 bar). The materials in the green box were selected for more refined screening and adsorbaphore identification; the colour-coding represents the number of MOFs according to the colour bar on the right. **b**, The H_2O affinity of the top-performing materials, as characterized by a plot of the Henry coefficients (K_H) for H_2O against those of CO_2. The colours represent the three different adsorbaphores found in the top-performing structures: A1, parallel aromatic rings; A2, metal–oxygen bridges; A3, open metal sites. Some materials have both A1 and A2 sites. **c**, The adsorbaphore containing parallel aromatic rings (A1), which was discovered using the feature-recognition algorithm.

106,680 such CO_2-binding sites (see Extended Data Fig. 3 for examples). A similarity analysis of these binding sites revealed three main classes of adsorbaphore: A1, two parallel aromatic rings with interatomic spacings of approximately 7 Å (31% of all binding sites); A2, metal–oxygen–metal bridges (32%); and A3, open metal sites (21%) (see Supplementary Information for details). Subsequently, we screened the materials that possessed these adsorbaphores for their affinity for water. Figure 1b shows the Henry coefficient for water in these high-performing materials. Analysis of the data shows that the materials with the parallel aromatic rings (A1) have a low Henry coefficient for H_2O, whereas those with metal–oxygen bridges (A2) and open metal sites (A3) tend to have higher Henry coefficients (Fig. 1b). A graphical representation of the different adsorbaphores is presented in Extended Data Fig. 4. Comparison of the binding energies—computed using density functional theory—for the adsorbaphore shown in Fig. 1c indicates a preference for CO_2 (−10.2 kcal mol^{-1}) over N_2 and H_2O by 2.7 and 1.5 kcal mol^{-1}, respectively (see Extended Data Table 1). The parallel aromatic rings provide a near-optimum interaction with all three atoms of CO_2, whereas for H_2O the lack of hydrogen-bonding sites limits its binding energy.

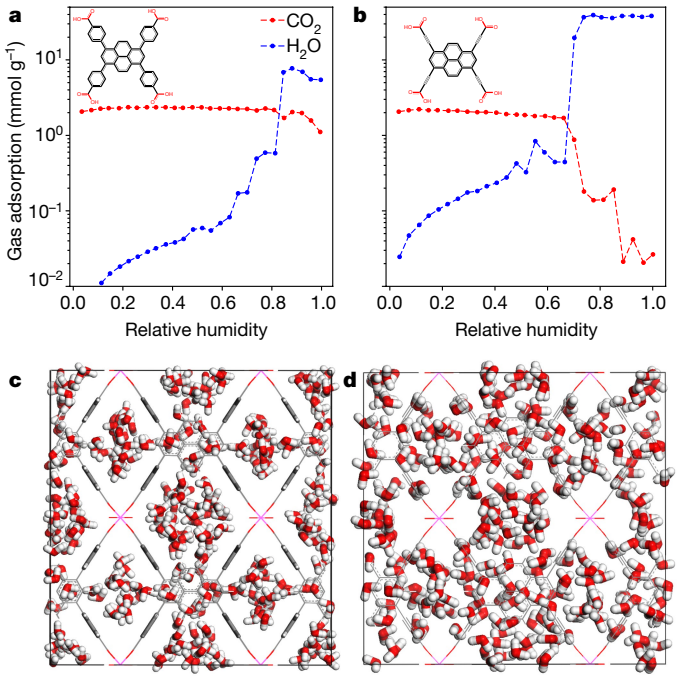


Fig. 2 | The effects of water on different MOFs with the same adsorbaphore. a, **b**, Simulated adsorption of a ternary mixture of $CO_2/N_2/H_2O$ at 313 K by hypothetical MOFs **m8o67** (**a**) and **m8o71** (**b**). The partial pressure of CO_2 was held at 0.15 bar as the relative humidity was increased. The N_2 uptake was negligible and is not shown. **c**, **d**, Visualization of the water loading at 100% relative humidity in **m8o67** (**c**) and **m8o71** (**d**). The benzoate groups are represented by grey sticks; water is shown using red and white space-filling atoms. In **m8o67**, the benzoate groups perpendicular to the plane of the figure prevent hydrogen-bond formation across the adsorbaphores.

The next step was to identify a subclass of MOFs in our library that contains the preferred adsorbaphore. From an experimental point of view, MOFs with the frz topology—characterized by tetra-carboxylated organic ligands coordinated to one-dimensional metal–oxygen rods—are an attractive starting point. One such example has been synthesized with indium as a metal node, resulting in a structurally stable, non-breathing MOF[18]. In this topology, the metal rods provide an ideal scaffolding to which we can attach our adsorbaphore. By varying the metal ion we have some flexibility to tune the distance between the aromatic rings. Our calculations predict that the ideal adsorbaphore distance of 6.5–7.0 Å—which was determined by adjusting the spacing of the aromatic rings incrementally (Extended Data Fig. 5)—can be approached if In(III) is replaced by Al(III) (Extended Data Table 2). In addition, aluminium is an attractive choice because it is an abundant metal and it ensures a strong bond with the carboxylate O-atoms of the ligands[19]; this considerably improves the thermal and hydrolytic stability of a MOF[20,21].

We generated a library of 35 isoreticular materials using our MOF-generation algorithm[22], and from the mixture isotherms we computed the

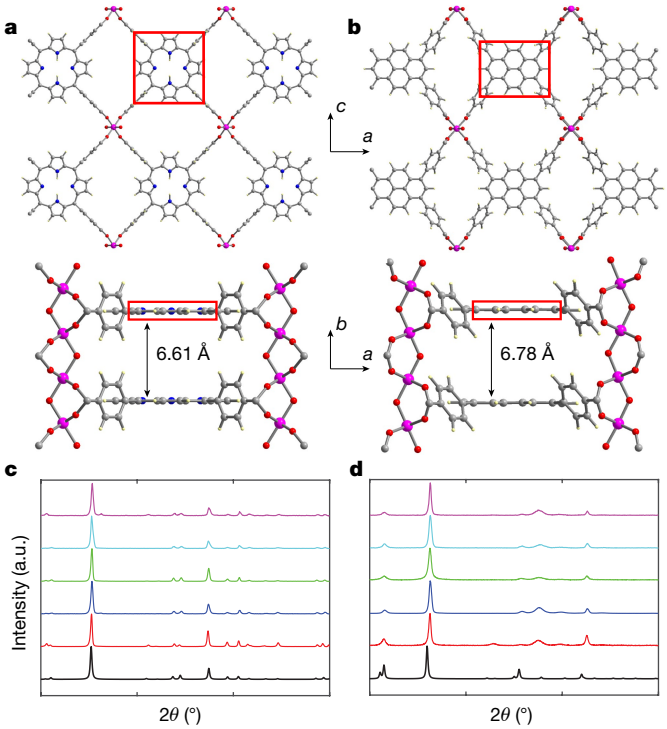


Fig. 3 | Structural representation and stability of [Al-PMOF] and [Al-PyrMOF]. a, **b**, Ball-and-stick representation of the structures of **[Al-PMOF]** (**a**) and **[Al-PyrMOF]** (**b**). The orientation of the tetracarboxylate ligands around the Al(III) rods results in the generation of the three-dimensional non-interpenetrated structures containing the adsorbaphore (red box). Atom colour code: pink, Al; grey, C; blue, N; red, O; pale yellow, H. **c**, **d**, Laboratory powder X-ray diffraction patterns of **[Al-PMOF]** (**c**) and **[Al-PyrMOF]** (**d**). Black, simulated; red, as-synthesized material; blue, acetone-exchanged material; green, activated material; sky blue, activated material immersed in liquid water for 7 days; pink, activated material exposed to a controlled atmosphere of nitric acid vapour for 3 h.

CO_2/N_2 selectivity of the materials in dry and wet flue gases (Extended Data Figs. 6 and 7). Our calculations show that all of our predicted materials maintain an excellent selectivity at low pressures, and in about 75% of these materials the selectivity was not influenced by the presence of water under flue-gas conditions. The concept of an adsorbaphore focuses on the design of an adsorption site that optimizes selectivities at low pressure. At higher partial pressures of water, its adsorption is dominated by the energetics of hydrogen-bond formation. Further analyses showed that, for the materials that maintain a high CO_2 uptake at high humidity, it is the pore shape that frustrates the formation of these hydrogen bonds. This is illustrated in Fig. 2a, b, which compares the effect of water on the CO_2 uptake of two materials that have the same adsorbaphore but different pore structures (hypothetical MOFs **m8o67** and **m8o71**). Figure 2a shows that **m8o67** is resistant to H_2O flooding: even at a relative humidity of approximately 85%, we find that H_2O has only a small effect on CO_2 capacity. Conversely, **m8o71** completely loses its CO_2 capacity at 60% relative humidity (Fig. 2b). In Fig. 2c, d we visualize the hydrogen-bond network that is formed at 100% relative humidity in both materials. For **m8o71** we see a complete hydrogen-bonding network (Fig. 2d), whereas for **m8o67** (Fig. 2c) we observe a less extensive network; the benzoate groups that separate the adsorbaphores frustrate the formation of a complete hydrogen-bonding network.

On the basis of these predictions, we synthesized two frz-based MOFs using organic ligands that possess the water-frustrating properties reported above: **Al-PMOF**[19] (**m8o66**) and **Al-PyrMOF** (**m8o67**). These MOFs are based on one-dimensional rods of Al(III) linked by TCPP (tetrakis(4-carboxyphenyl)porphyrin) and TBAPy (1,3,6,8-tetrakis (*p*-benzoic acid)pyrene) ligands, respectively (Fig. 3a, b). Figure 3c, d shows no loss of crystallinity upon activation as well as upon exposure to different harsh conditions, including immersion in water for 7 days.

By identifying adsorbaphores in these hypothetical materials, we assume that our in silico screening method can correctly predict the structure of a MOF, its adsorption properties, and the nature of the binding sites of CO_2 and H_2O. We are able to test these assumptions for **Al-PMOF** and **Al-PyrMOF**. In Fig. 4a we show that the experimental and predicted CO_2 and N_2 adsorption isotherms are in good agreement. The CO_2 binding positions in the adsorbaphore and the effect of H_2O are more challenging to observe experimentally. The siting of CO_2 was studied using in situ CO_2-loading powder X-ray diffraction. Upon loading, we observed a considerable change in the intensity and peak position of the Bragg reflections (see Supplementary Fig. 2.1). Subsequent Rietveld refinement and Fourier analysis[23] revealed the preferred locations of CO_2 in the pores of **Al-PMOF**, as shown in Fig. 4b. These results confirm that CO_2 preferentially adsorbs in the adsorbaphore.

The effect of water on the siting of CO_2 has been further addressed by solid-state nuclear magnetic resonance (NMR) analysis. Under magic-angle spinning (MAS), high-resolution ^{13}C NMR chemical shifts are very sensitive to changes in the chemical environment. The ^{13}C NMR spectra of **Al-PyrMOF** and **Al-PMOF** are provided in Extended Data Fig. 8, which also shows the assignment of the peaks to specific atoms on the MOF. The chemical shifts associated with the atoms of the adsorbophore (inset) are shown in Fig. 4c as a function of the water concentration. At low levels the adsorbophore atoms experience no change in chemical environment with water loading, whereas at the highest water loadings there are modest changes in the carbon-13 chemical shifts of only those atoms that are close to the aluminium-coordinated carboxylate groups next to the adsorbaphore (carbons B and F in Fig. 4c). This broadening is consistent with dipolar broadening from proximate water molecules, thus confirming that the adsorbaphore itself is not a preferential adsorption site for H_2O.

Our simulations predict that CO_2 adsorbed in the adsorbaphore is insulated from the adsorption of water. Because the ^{13}C NMR spectrum of adsorbed $^{13}CO_2$ is extremely sensitive to the proximity of water molecules in terms of chemical shift and line broadening, any disruption of the chemical environment of adsorbed CO_2 by water should be immediately apparent. Figure 4d shows that the chemical shift of the adsorbed $^{13}CO_2$ is independent of water content, although a broadening of the ^{13}C NMR peak is observed with increasing humidity. If this broadening is due to the proximity of the protons in water, it should disappear if the experiments are repeated using D_2O; however, it does not (Fig. 4d). This observation corroborates our simulation results (Fig. 2c), confirming that water has only a limited effect on CO_2 adsorption in **Al-PyrMOF**.

The ability of these materials to capture CO_2 from wet flue gases is of important practical concern. We therefore used a breakthrough experiment to determine the capture capacity of both **Al-PMOF** and **Al-PyrMOF** for a mixture of CO_2/N_2 under dry- and humid-conditions[24] (Fig. 4e). These results confirm the predictions of the simulations (Extended Data Fig. 7): humidity in the flue gases has only a minimal influence on the capture capacity of **Al-PMOF**, whereas for **Al-PyrMOF** the capture capacity is in fact enhanced. Furthermore, repeated cycling[25] (Fig. 4f) does not result in degradation of the material or a change in separation performance. It is instructive to compare the performance of our materials with that of a set of reference materials, including those that are commercially available—such as zeolite 13X and activated carbon—and a water stable, amino-functionalized MOF, UiO-66-NH_2. The capture capacity of these reference materials lies between that of **Al-PyrMOF** and **Al-PMOF** in dry flue gases; however, unlike our MOFs, their performance reduces considerably in humid flue gases. Although our materials do not have the highest reported

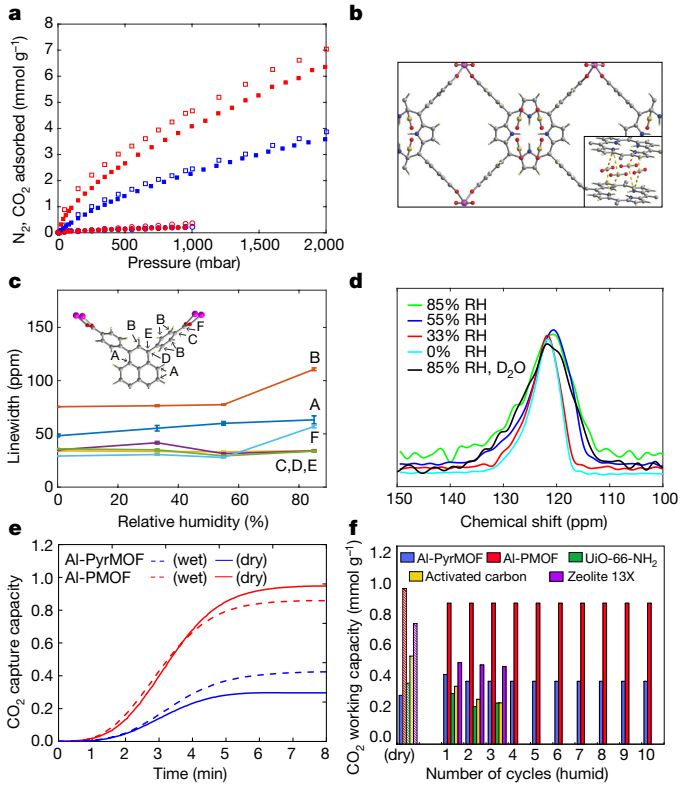


Fig. 4 | CO_2 adsorption, ^{13}C cross-polarization MAS NMR and breakthrough experiments for [Al-PMOF] and [Al-PyrMOF]. **a**, Experimental (filled) and computational (open) single-component adsorption isotherms for CO_2 (squares) and N_2 (circles) adsorption collected on activated **[Al-PMOF]** (red) and **[Al-PyrMOF]** (blue) at 313 K. **b**, Rietveld refinement of the X-ray diffraction data (Supplementary Information) revealed that CO_2 binding in **[Al-PMOF]** occurs between the porphyrin cores—that is, in the adsorbaphore. **c**, The linewidth of each carbon peak of the TBAPy ligand in **[Al-PyrMOF]** in the ^{13}C cross-polarization MAS spectrum, plotted as a function of relative humidity. Each carbon atom in the ligand is labelled in the inset. **d**, Linewidths extracted from the ^{13}C static NMR spectra of $^{13}CO_2$ loaded in **[Al-PyrMOF]**, plotted against relative humidity (RH). **e**, CO_2 capture capacity profiles for **[Al-PyrMOF]** and **[Al-PMOF]** during breakthrough experiments under dry and humid (85% relative humidity) conditions, with 85/15 v/v of N_2/CO_2 (313 K and 1 bar). **f**, Benchmarking the CO_2 working capacity of **[Al-PyrMOF]** and **[Al-PMOF]** against UiO-66-NH_2, activated carbon and zeolite 13X under dry and humid (85% relative humidity) conditions, with 85/15 v/v of N_2/CO_2 (313 K and 1 bar). For wet flue gases, we studied the performance stability after 3 cycles for reference materials, and after 10 cycles for **[Al-PyrMOF]** and **[Al-PMOF]**.

working capacities[14], it is encouraging to see that, in wet flue gases, **Al-PMOF** outperforms commercial materials such as zeolite 13X and activated carbon.

Large-scale screening of databases of hypothetical MOFs for various gas separation and storage applications has been reported previously[26–29]; however, here we have focused on identifying binding pockets—or structural motifs termed adsorbaphores—as synthetic targets, rather than whole materials. This enhances the synthetic viability of the approach, as demonstrated by the identification of one new material with the targeted adsorbaphore that was synthesized and shown to adsorb CO_2 as predicted. The concept of linking computational screening with the synthesis of the corresponding materials through such adsorbaphores should be applicable to other gas separations of increasing complexity.

Online content

Any methods, additional references, Nature Research reporting summaries, source data, extended data, supplementary information, acknowledgements, peer review information; details of author contributions and competing interests are available at https://doi.org/10.1038/s41586-019-1798-7.

1. Smit, B., Reimer, J. R., Oldenburg, C. M. & Bourg, I. C. *Introduction to Carbon Capture and Sequestration* (Imperial College Press, 2014).
2. Bui, M. et al. Carbon capture and storage (CCS): the way forward. *Energy Environ. Sci.* **11**, 1062–1176 (2018).
3. D'Alessandro, D. M., Smit, B. & Long, J. R. Carbon dioxide capture: prospects for new materials. *Angew. Chem. Int. Ed.* **49**, 6058–6082 (2010).
4. Sumida, K. et al. Carbon dioxide capture in metal–organic frameworks. *Chem. Rev.* **112**, 724–781 (2012).
5. Furukawa, H., Cordova, K. E., O'Keeffe, M. & Yaghi, O. M. The chemistry and applications of metal–organic frameworks. *Science* **341**, 1230444 (2013).
6. Huck, J. M. et al. Evaluating different classes of porous materials for carbon capture. *Energy Environ. Sci.* **7**, 4132–4146 (2014).
7. Mason, J. A., Sumida, K., Herm, Z. R., Krishna, R. & Long, J. R. Evaluating metal–organic frameworks for post-combustion carbon dioxide capture via temperature swing adsorption. *Energy Environ. Sci.* **4**, 3030–3040 (2011).
8. Li, G. et al. Capture of CO_2 from high humidity flue gas by vacuum swing adsorption with zeolite 13X. *Adsorption* **14**, 415–422 (2008).
9. Merel, J., Clausse, M. & Meunier, F. Experimental investigation on CO_2 post-combustion capture by indirect thermal swing adsorption using 13X and 5A zeolites. *Ind. Eng. Chem. Res.* **47**, 209–215 (2008).
10. Milner, P. J. et al. A diaminopropane-appended metal–organic framework enabling efficient CO_2 capture from coal flue gas via a mixed adsorption mechanism. *J. Am. Chem. Soc.* **139**, 13541–13553 (2017).
11. McDonald, T. M. et al. Cooperative insertion of CO_2 in diamine-appended metal–organic frameworks. *Nature* **519**, 303–308 (2015).
12. Flaig, R. W. et al. The chemistry of CO_2 capture in an amine-functionalized metal–organic framework under dry and humid conditions. *J. Am. Chem. Soc.* **139**, 12125–12128 (2017).
13. Couck, S. et al. An amine-functionalized MIL-53 metal–organic framework with large separation power for CO_2 and CH_4. *J. Am. Chem. Soc.* **131**, 6326–6327 (2009).
14. Chanut, N. et al. Screening the effect of water vapour on gas adsorption performance: application to CO_2 capture from flue gas in metal–organic frameworks. *ChemSusChem* **10**, 1543–1553 (2017).
15. Wolber, G., Seidel, T., Bendix, F. & Langer, T. Molecule-pharmacophore superpositioning and pattern matching in computational drug design. *Drug Discov. Today* **13**, 23–29 (2008).
16. Sliwoski, G., Kothiwale, S., Meiler, J. & Lowe, E. W., Jr. Computational methods in drug discovery. *Pharmacol. Rev.* **66**, 334–395 (2013).
17. Ho, M. T., Allinson, G. W. & Wiley, D. E. Reducing the cost of CO_2 capture from flue gases using pressure swing adsorption. *Ind. Eng. Chem. Res.* **47**, 4883–4890 (2008).
18. Stylianou, K. C. et al. A guest-responsive fluorescent 3D microporous metal–organic framework derived from a long-lifetime pyrene core. *J. Am. Chem. Soc.* **132**, 4119–4130 (2010).
19. Fateeva, A. et al. A water-stable porphyrin-based metal–organic framework active for visible-light photocatalysis. *Angew. Chem. Int. Ed.* **51**, 7440–7444 (2012).
20. Loiseau, T. et al. A rationale for the large breathing of the porous aluminum terephthalate (MIL-53) upon hydration. *Chem. Eur. J.* **10**, 1373–1382 (2004).
21. Reinsch, H. & Stock, N. High-throughput studies of highly porous Al-based MOFs. *Microporous Mesoporous Mater.* **171**, 156–165 (2013).
22. Boyd, P. G. & Woo, T. K. A generalized method for constructing hypothetical nanoporous materials of any net topology from graph theory. *CrystEngComm* **18**, 3777–3792 (2016).
23. Carrington, E. J., Vitórica-Yrezábal, I. J. & Brammer, L. Crystallographic studies of gas sorption in metal–organic frameworks. *Acta Crystallogr. B* **70**, 404–422 (2014).
24. García, S. et al. Breakthrough adsorption study of a commercial activated carbon for pre-combustion CO_2 capture. *Chem. Eng. J.* **171**, 549–556 (2011).
25. García, S., Gil, M. V., Pis, J. J., Rubiera, F. & Pevida, C. Cyclic operation of a fixed-bed pressure and temperature swing process for CO_2 capture: experimental and statistical analysis. *Int. J. Greenhouse Gas Control* **12**, 35–43 (2013).
26. Lin, L.-C. et al. In silico screening of carbon-capture materials. *Nat. Mater.* **11**, 633–641 (2012).
27. Wilmer, C. E. et al. Large-scale screening of hypothetical metal–organic frameworks. *Nat. Chem.* **4**, 83–89 (2012).
28. Boyd, P. G., Lee, Y. & Smit, B. Computational development of the nanoporous materials genome. *Nat. Mater. Rev.* **2**, 17037 (2017).
29. Yazaydin, A. O. et al. Screening of metal–organic frameworks for carbon dioxide capture from flue gas using a combined experimental and modeling approach. *J. Am. Chem. Soc.* **131**, 18198–18199 (2009).

Publisher's note Springer Nature remains neutral with regard to jurisdictional claims in published maps and institutional affiliations.

© The Author(s), under exclusive licence to Springer Nature Limited 2019

Data availability

The computed data and hypothetical materials that were used in this Article are provided free of charge on the Materials Cloud (https://doi.org/10.24435/materialscloud:2018.0016/v3). An interactive version of Fig. 1a, b can also be found on this site. Data that are not included in the paper are available upon reasonable request to the corresponding authors.

Code availability

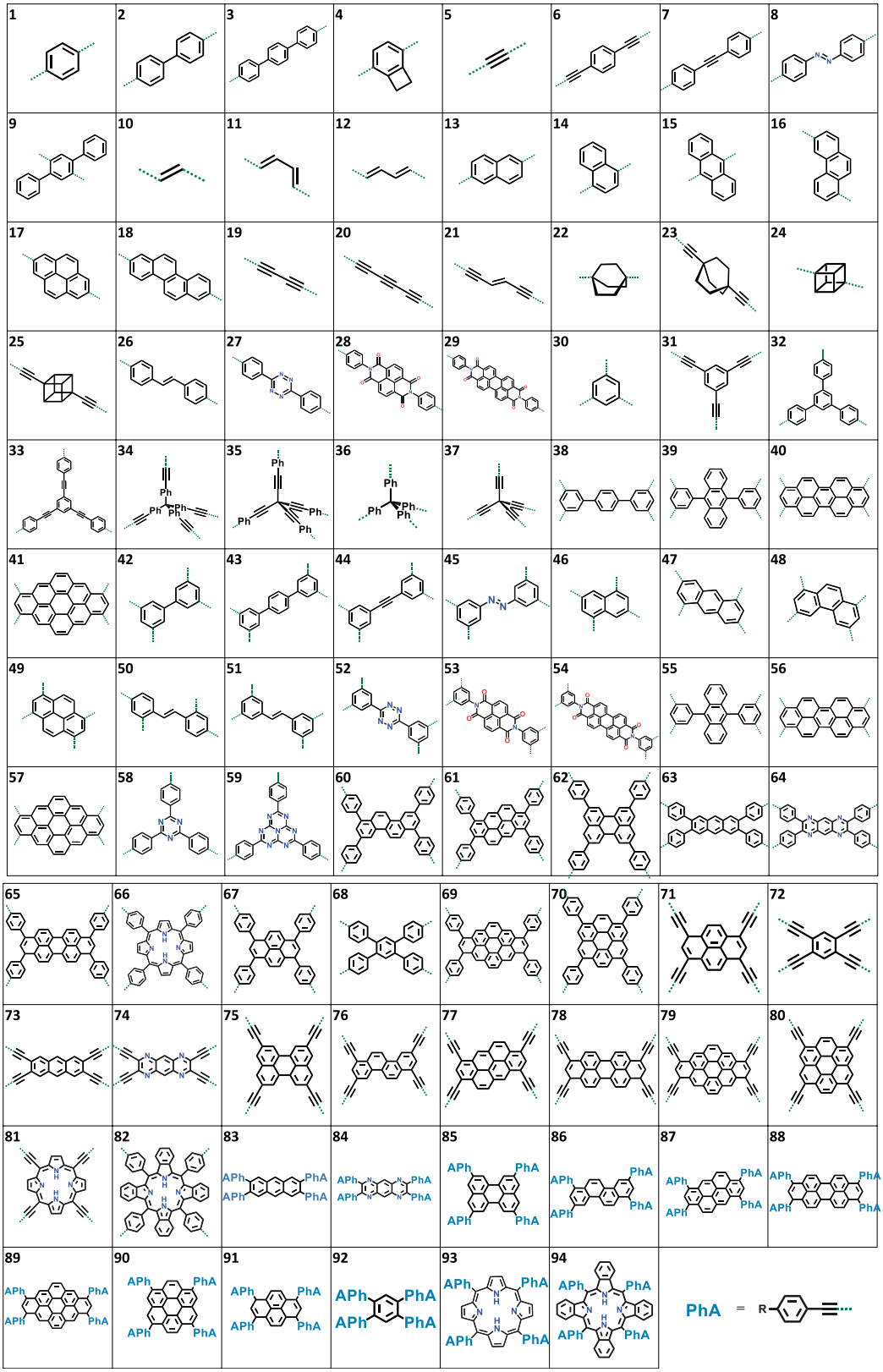
Topology Based Crystal Constructor (ToBasCCo), the Python program used to build hypothetical MOFs, is hosted on GitHub at https://github.com/peteboyd/tobascco. The Python code that compares common chemical features between fragments is also provided on GitHub at https://github.com/peteboyd/adsorbaphore and is dependent on a C library called MCQD which performs the maximum clique detection of the chemical graphs. An interface between Python and C for this is provided here at https://github.com/peteboyd/mcqd_api. The Automatic Binding Site Locator (ABSL) program, used to identify CO_2 binding sites in each MOF, is part of a broader Python-based code used to facilitate simulations of porous materials called Fully Automated Adsorption Analysis in Porous Solids (FA^3PS). This is available on BitBucket at https://bitbucket.org/tdaff/automation.

Acknowledgements K.C.S. was supported by the Swiss National Science Foundation (SNF) under the Ambizione Energy Grant n.PZENP2_166888, P.G.B. and B.S. by the European Research Council (ERC) Advanced Grant (grant agreement no. 666983, MaGic) and the National Center of Competence in Research (NCCR), Materials' Revolution: Computational Design and Discovery of Novel Materials (MARVEL). A.C., C.P.I., and S.M.M. were supported by European Union's Horizon 2020 research and innovation programme under grant agreement no. 760899 (GENESIS). R.B. and J.A.R. were supported by the Center for Gas Separations Relevant to Clean Energy Technologies, an Energy Frontier Research Center funded by the Department of Energy (DOE), Office of Science, Office of Basic Energy Sciences under award DE-SC0001015. E.G.-D. is supported by the European Commission under the Research Fund for Coal and Steel (RFCS) Programme (project no. 709741). M.M.M.-V. and S.G. acknowledge the financial support from the Engineering and Physical Sciences Research Council (EP/N024540/1) and the Research Centre for Carbon Solutions (RCCS) at Heriot-Watt University. The authors thank the Swiss Norwegian Beamlines of ESRF for beamtime allocation at BM31 for the in-situ CO_2 loading and variable temperature powder X-ray diffraction experiments. This work was supported by a grant from the Swiss National Supercomputing Center (CSCS) under project no. s761, as well as resources from the National Energy Research Scientific Computing Center, a DOE Office of Science User Facility supported by the Office of Science of the US Department of Energy under contract no. DE-AC02-05CH11231. J.A.R.N. acknowledges Spanish MINECO (CTQ2017-84692-R) and EU Feder funding. P.G.B., T.D.D. and T.K.W. would like to thank NSERC of Canada for financial support and Compute Canada for computing resources. S.G., J.A.R., and B.S. acknowledge support during the final stage of the work of the ACT-PrISMa project, which has received joint funding from BEIS, NERC and EPSRC (UK), funding from the Division of CCS R&D, US Department of Energy (USA), and funding from the Office Fédéral de l'Energie (Switzerland).

Author contributions P.G.B. and T.K.W. developed the adsorbaphore similarity algorithm and developed the library of hypothetical MOFs. P.G.B., T.K.W. and B.S. characterised the adsorbaphores; T.D.D. carried out the initial computational screening and developed the MOF-CO_2 binding site identification algorithm. S.M.M. carried out the pore similarity analysis; A.C., C.P.I. and K.C.S. synthesized and characterized the materials. The breakthrough experiments were carried out by E.G.-D., C.P.I., A.C., M.M.M.-V., J.A.R.N. and S.G. The NMR experiments were carried out by R.B. and J.A.R; X-ray analysis was carried out by A.G. and P.S. All authors contributed to the analysis of the data and the writing of the manuscript.

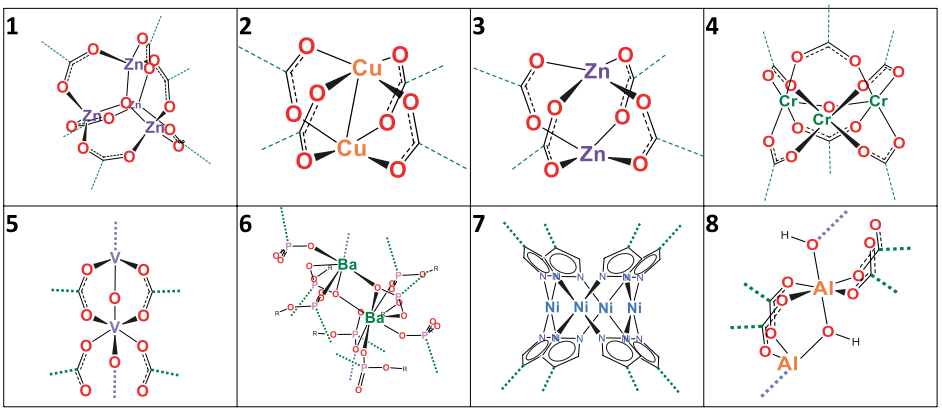
Competing interests K.C.S., B.S., A.C., P.G.B. and T.K.W. have filed an international patent application (no. 18 168 544.7) that relates to water-stable polyaromatic MOF materials for CO_2 separation from flue gas and natural gas streams.

Additional information
Supplementary information is available for this paper at https://doi.org/10.1038/s41586-019-1798-7.
Correspondence and requests for materials should be addressed to T.K.W., S.G., K.C.S. or B.S.
Peer review information *Nature* thanks Philip Llewellyn and the other, anonymous, reviewer(s) for their contribution to the peer review of this work.
Reprints and permissions information is available at http://www.nature.com/reprints.

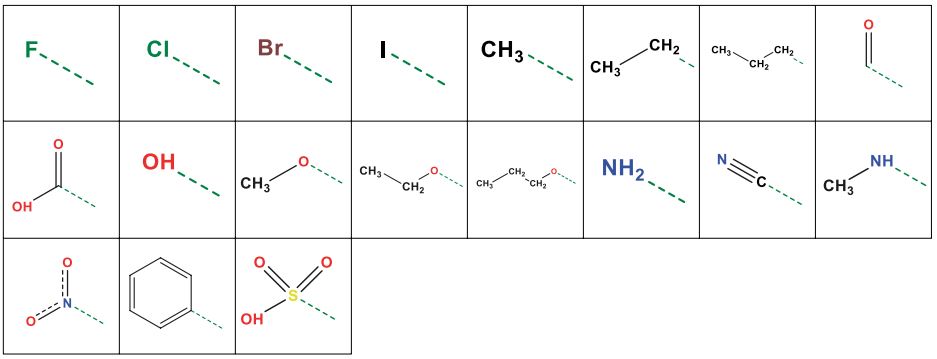


Extended Data Fig. 1 | Hypothetical material generation (1). The organic secondary building units (SBUs) used in the generation of the hypothetical MOF database.

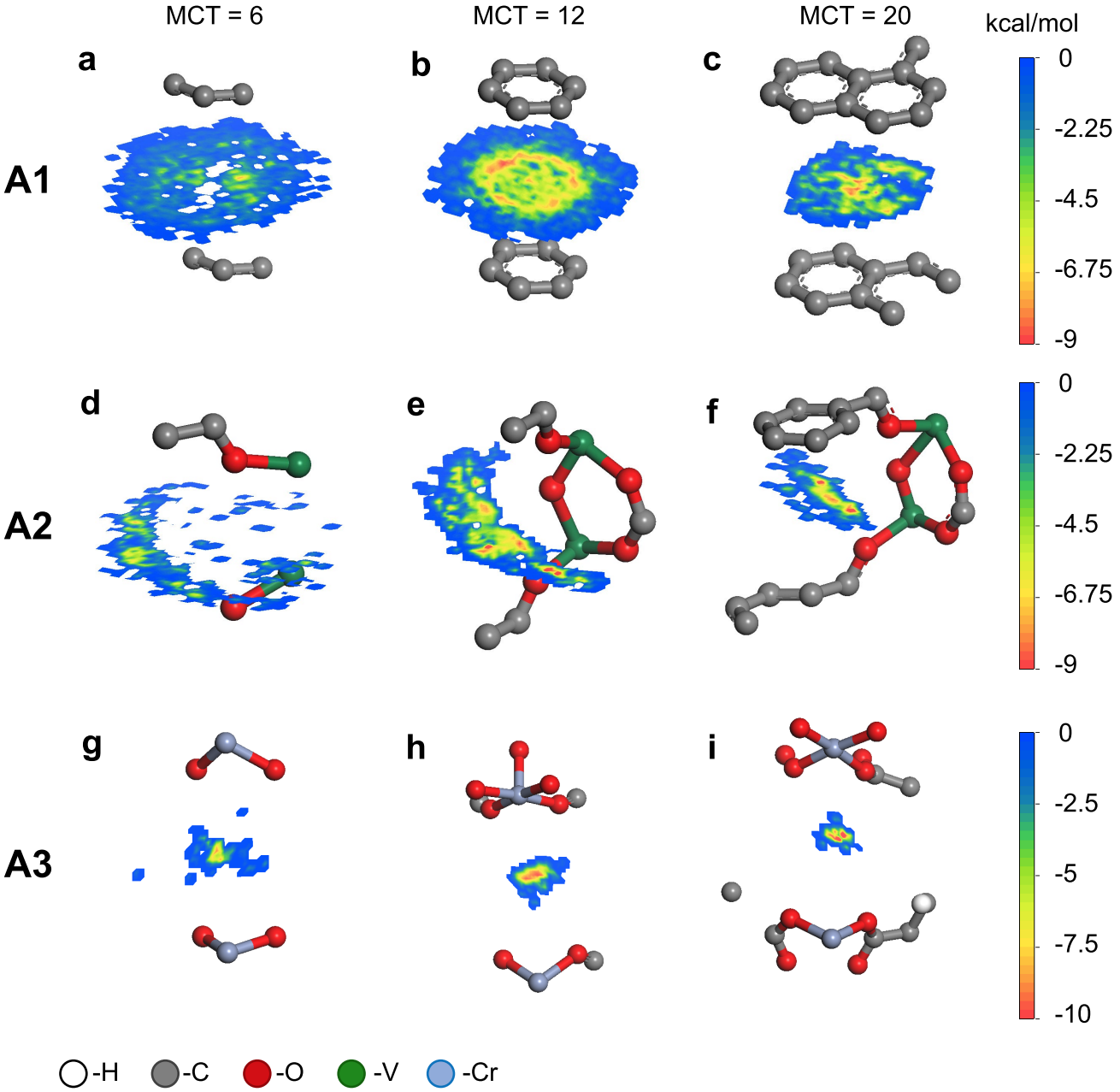
a



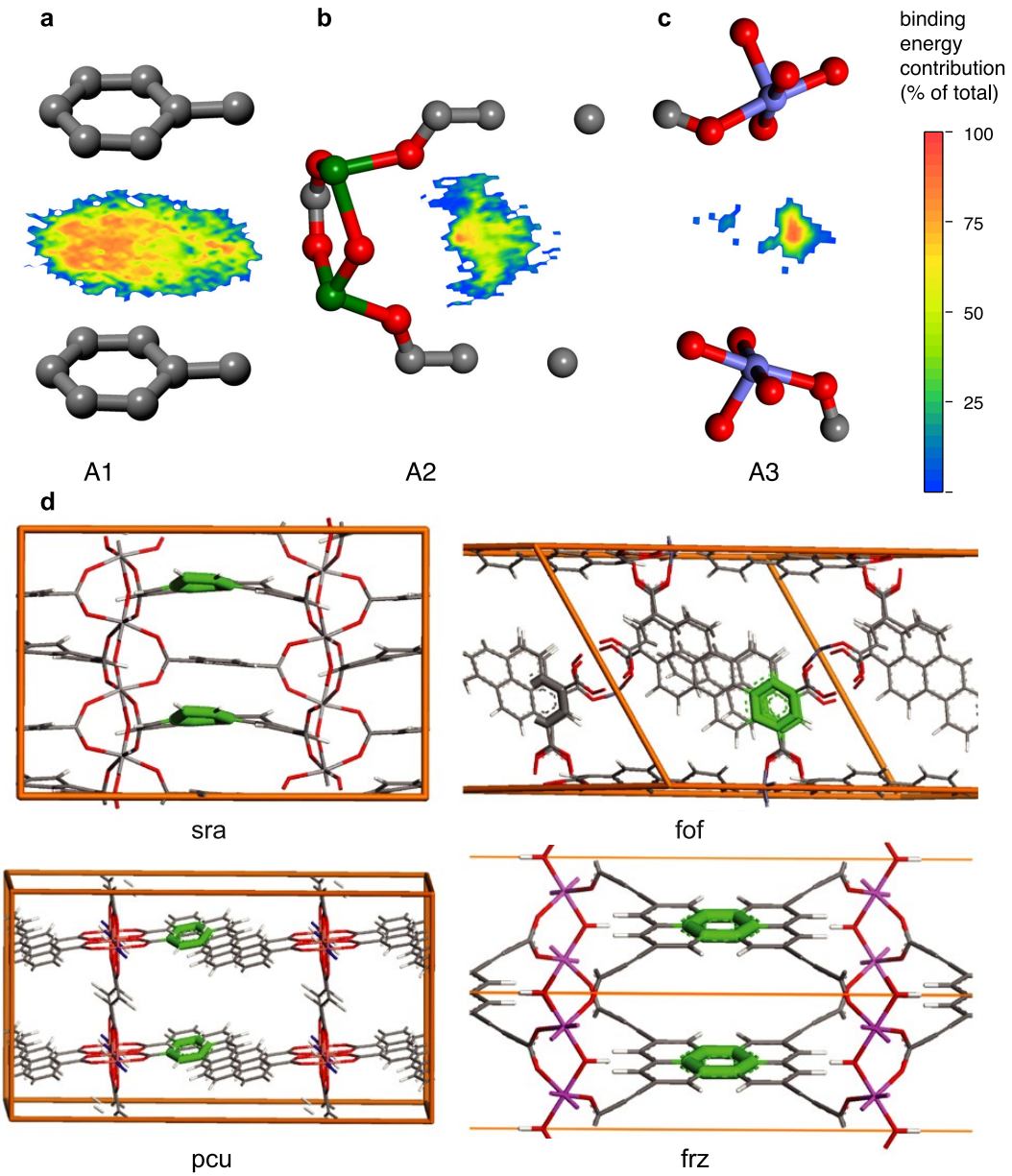
b



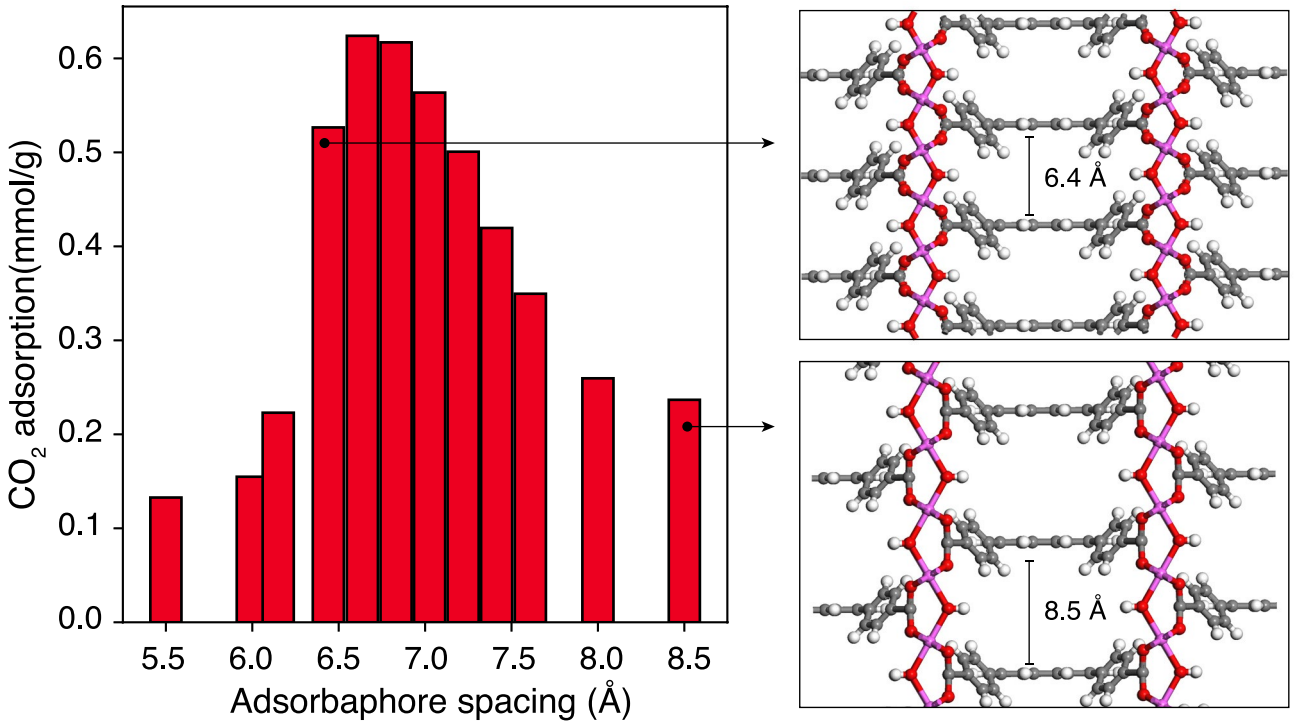
Extended Data Fig. 2 | Hypothetical material generation (2). a, Metal SBUs used in the generation of the hypothetical MOF database. **b**, Functional groups used to decorate the unfunctionalized hypothetical MOFs in the database. We denote a hypothetical material as **mXoYY**, where X refers to the metal SBU shown in **a** and YY refers to the organic SBU shown in Extended Data Fig. 1. Functional groups were decorated onto the base hypothetical materials using an internal numbering system.



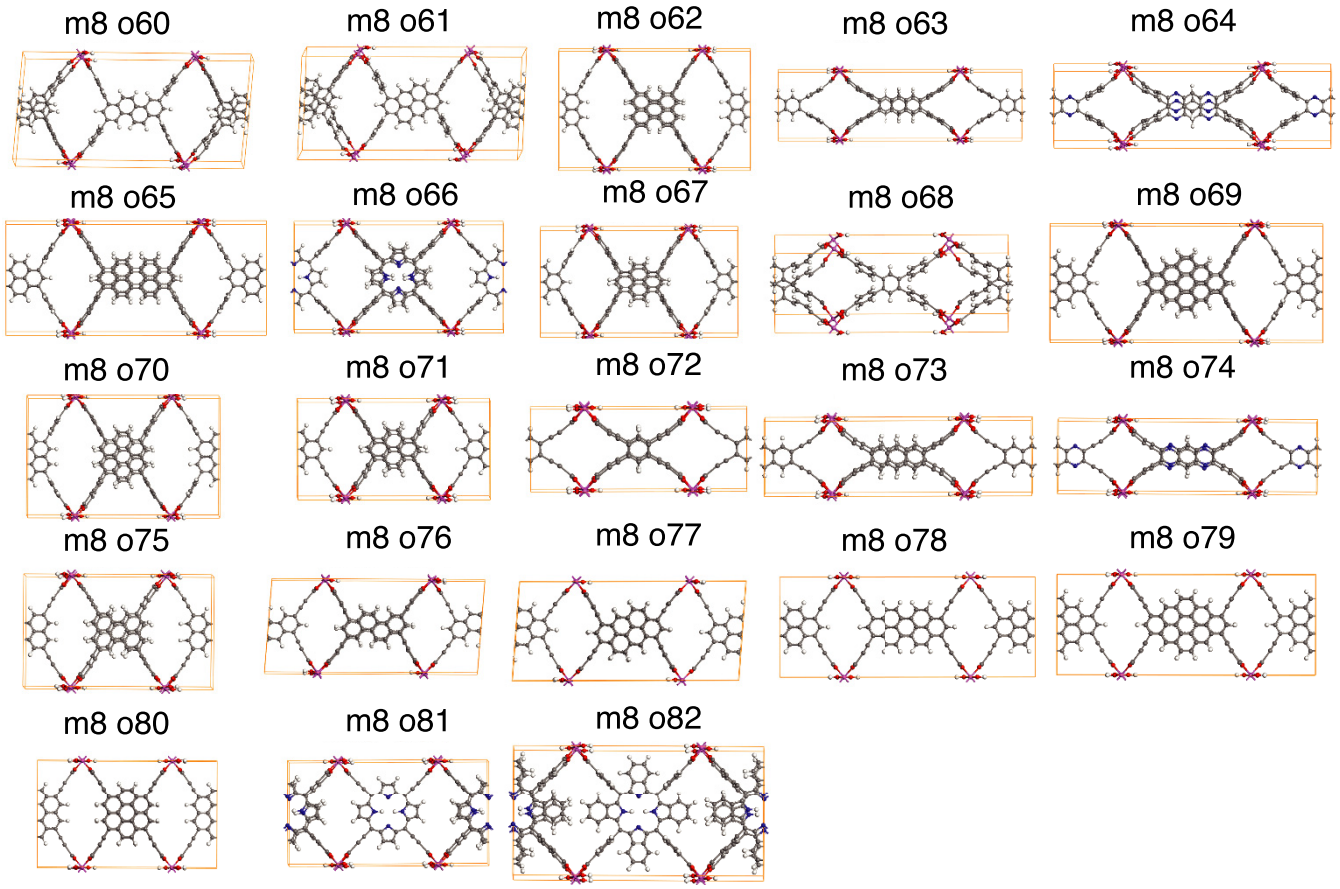
Extended Data Fig. 3 | Examples of adsorbaphores. A selection of the most representative adsorbaphores obtained from visual inspection of the top 50 most frequent adsorbaphores found from the random pairing method described in the Supplementary Information. There are three major trends in the molecular fragments—labelled A1, A2 and A3—which can be observed upon descending each column. The number of chemical features of the fragments increases from left to right across each row. This is accomplished by increasing the minimum number of common atoms allowed during the substructure search, called the minimum clique threshold (MCT). Pictured in each adsorbaphore is a representative contour map of the energy produced from CO_2 binding with the adsorbaphore atoms from each original CO_2-binding site. **a**–**c**, A1, planar aromatic systems, in which CO_2 binds in between the stacked rings; **d**–**f**, A2, CO_2 binds near the bridging oxygen of a pillared vanadium SBU; **g**–**i**, A3, CO_2 binds between open-metal Cr SBUs.



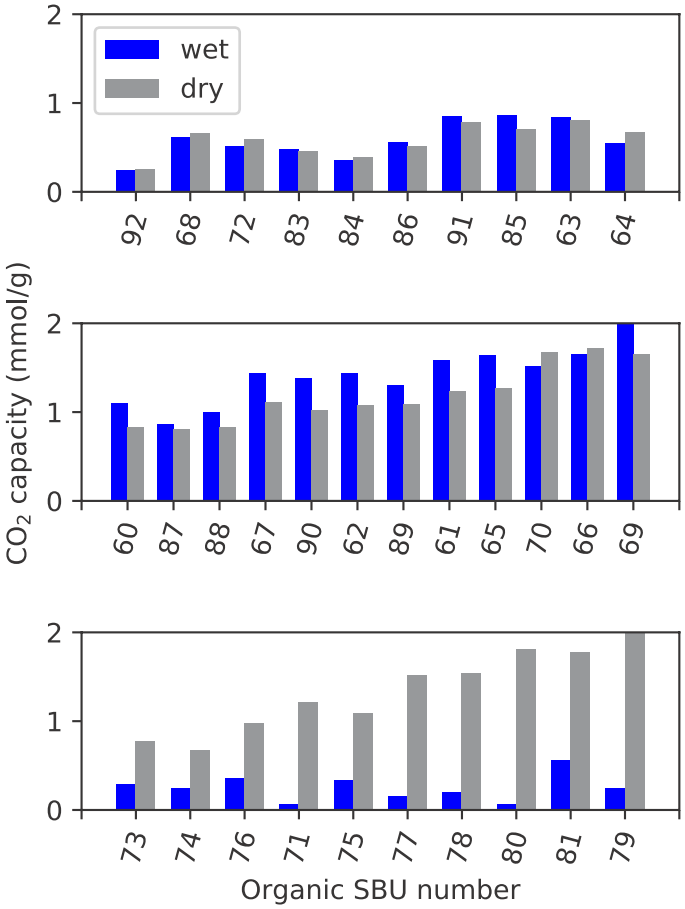
Extended Data Fig. 4 | Frequently found adsorbaphores. a–**c**, Frequently found adsorbaphores from the maximum clique detection method; A1 (**a**); A2 (**b**) and A3 (**c**). Atom colours: grey, carbon; red, oxygen; green, vanadium; blue, chromium. **d**, Representative adsorbaphore A1 found in different hypothetical MOFs from the hypothetical database. The adsorbaphore atoms are highlighted in green.



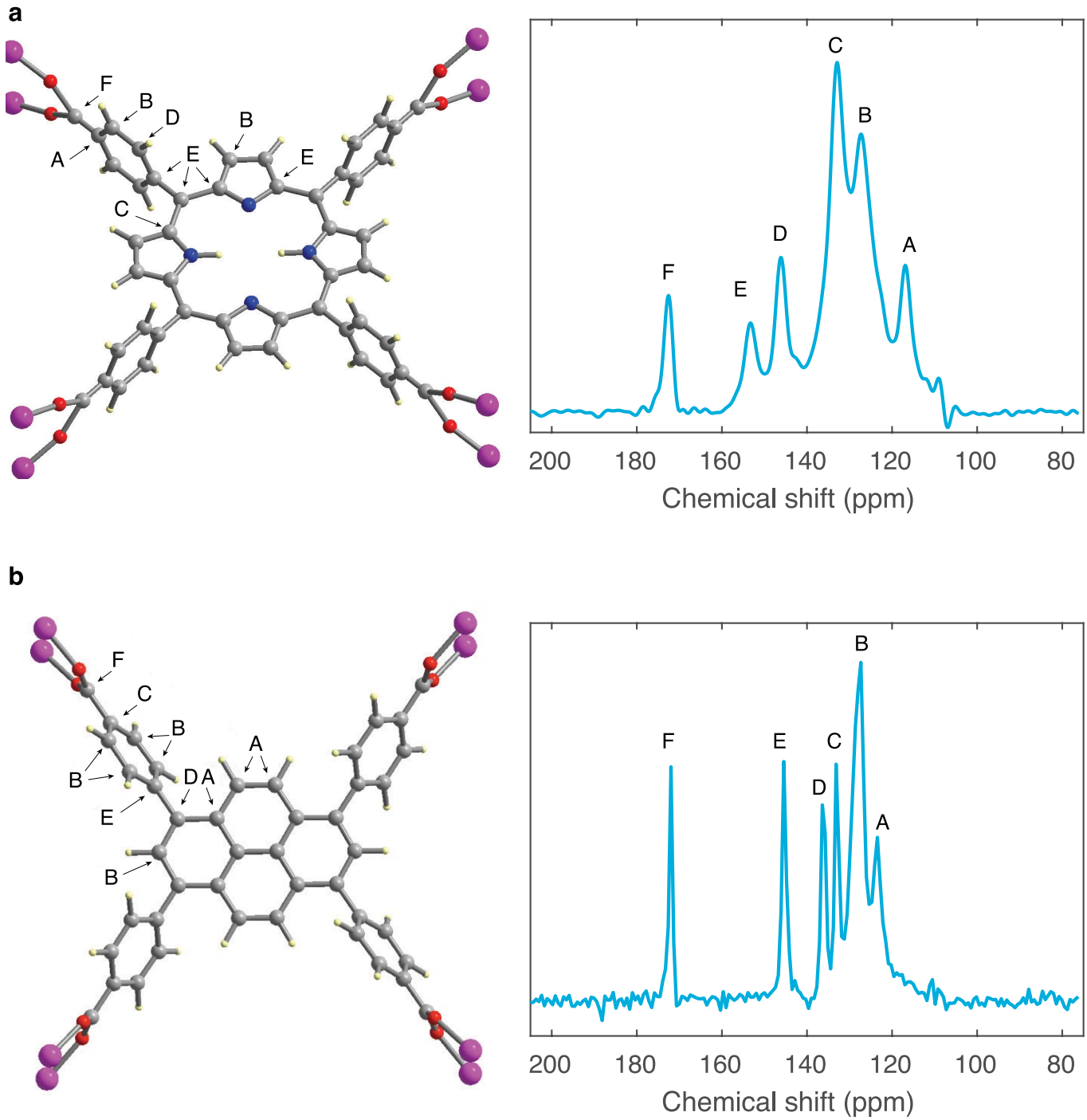
Extended Data Fig. 5 | Effect of the adsorbaphore spacer. Left, plot of the CO_2 adsorption at 0.15 bar and 313 K in hypothetical MOFs with the frz topology, metal node number 8 and organic linker number 67 (m8o67). The interplanar spacing of the adsorbaphore atoms is adjusted by reassembling the structure with longer or shorter Al–O bonds. Right, representation of the spacing adjustments made to the material.



Extended Data Fig. 6 | Hypothetical MOFs built with the frz topology. These structures contain an Al one-dimensional rod (m8) and the organic ligands 60–82 from Extended Data Figs. 1 and 2. The spacing between parallel aromatic cores (seen in the centre of each hypothetical MOF) is around 6.7 Å, defining the adsorbaphore site in each material. No functional groups were used to decorate these materials. We refer to the synthesized versions of **m8o66** and **m8o67** as **Al-PMOF** ($Al_2(OH)_2(H_2TCPP)$) and **Al-PyrMOF** ($Al_2(OH)_2(TBAPy)$), respectively.



Extended Data Fig. 7 | CO_2 adsorption capacity of a class of frz-based hypothetical MOFs at 0.15 bar and 313K under 'wet' (85% relative humidity) and 'dry' flue gas conditions. Top, middle, hypothetical MOFs in which the organic ligand is connected to the Al ion via 4 benzoate moieties; bottom, hypothetical MOFs in which the organic ligand is connected to the Al metal ion via 4 acetylenic carboxylate moieties. The materials are ranked from lowest adsorbaphore density to highest, and the number on the *x* axis corresponds to the organic linker number (YY) in m8oYY (see Extended Data Fig. 6).



Extended Data Fig. 8 | NMR spectra. a, **b**, ^{13}C cross-polarization MAS spectrum of **Al-PMOF** (**a**) and **Al-PyrMOF** (**b**) recorded at 9.39 T with sample spinning at 8 kHz; the contact time for the cross-polarization experiment was 2 ms. The letters labelling the peaks of the spectra correspond to the labels on the carbon atoms in the structures on the left.

Extended Data Table 1 | DFT binding energies of gas particles in the adsorbaphore pocket of each MOF synthesized in this work

MOF	Adsorbaphore Binding Energy (kcal/mol)		
	CO_2	H_2O	N_2
Al-PMOF	-12.6	-10.4	-7.9
Al-PyrMOF	-10.2	-8.7	-7.5

Extended Data Table 2 | DFT optimized cell parameters of hypothetical MOFs

Metal species	*a* (Å)	*b* (Å)	**c (Å)**
Al(III)	15.84	30.33	**6.65**
Fe(III)	15.96	30.47	**6.83**
Ga(III)	15.97	30.56	**6.77**
In(III)	16.23	30.88	**7.27**
Sc(III)	16.12	30.70	**7.34**
Y(III)	16.43	30.72	**7.70**

The MOFs are built with the frz topology and organic linker number 67 (m8o67) and various trivalent metal species. The c axis corresponds to the spacing between aromatic rings in the adsorbaphore.